ISABE-2015-20109

EFFECT OF ATTACK ANGLE AND JET HEIGHT ON IMPINGEMENT AND FILM COMPOSITE COOLING OF TURBINE BLADE LEADING EDGE

Zhao Liu, Lv Ye, Xing Yang, Zhenping Feng*

Institute of Turbomachinery, School of Energy and Power Engineering,
Xi'an Jiaotong University, Xi'an, Shaanxi, 710049, P.R. China

(*Corresponding Authors: zpfeng@mail.xjtu.edu.cn)

Abstract

In this paper numerical simulation is performed to simulate the impingement and film composite cooling on blade leading edge region. The relative performances of turbulence models are compared with available experimental data, and results show that SST *k-ω* model is the best based on simulation accuracy. Then the SST *k-ω* model is adopted for this study. Grid independence study is also carried out by using the Richardson extrapolation method. A single array of circle jets and three rows of film holes are arranged to investigate the impingement and film composite cooling. Five different values of main stream attack angles and five different values of flat portion to jet nozzle diameter ratios are studied in detail. The results indicate that heat transfer coefficient on the internal surface of turbine blade leading edge slightly changes with mainstream attack angle, but external film cooling effectiveness distribution would vary rapidly with mainstream attack angle. And with an increase in flat portion to jet nozzle diameter ratios, heat transfer coefficient on blade leading edge internal surface decreases, while external film cooling effectiveness distribution barely changes.

Keywords: Blade leading edge, Attack angle, Jet height, Impingement cooling, Film cooling

Nomenclature

B	Width of equivalent slot jet used in Ref. [5] [mm]
C	Hole spacing of each row [mm]
D	Diameter [mm]
H	Jet from target surface [mm]
h	Heat transfer coefficient [W/(m^2·K)]
L	Length of flat portion [mm]
M	Average blowing ratio
Nu	Nusselt number
P	Pressure [Pa]
q	Heat flux [W/m^2]
*r**	Ratio of curvature radius to of semi-cylindrical airfoil radius used in Ref. [5]
Re	Reynolds number
S	Streamwise coordinate [mm]
V	Velocity [m/s]
T	Temperature [K]
Y	Transverse coordinates from wall (m)
y$^+$	Non-dimensional distance, =Y u_τ/ν
η	Cooling effectiveness
ρ	Density [kg/m^3]
α	Angle of the second row of film holes from the stagnation line [°]
β	Angle of film holes from the surface in spanwise [°]
γ	Attack angle of main flow [°]
u_τ	Shear velocity (m/s)
ν	Kinematic viscosity (m^2/s)

subscripts

av	Average
aw	Adiabatic wall
c	Coolant
f	Film hole
i	Inlet
ip	Impingement hole
sp	Spanwise-averaged
w	Wall
o	Outlet
∞	Mainstream
1,2	Film hole number

1 Introduction

In order to enhance the turbine efficiency and power, modern gas turbine systems are required to operate at higher and higher temperature, and thus turbine components are suffering the increasing heat loads. As a result, turbine inlet temperature has already been far beyond the material acceptable level. Then the leading edge area of gas turbine blade will have a higher heat flux as it is upwind to high temperature inflows. A series of cooling technologies such as impingement cooling, film cooling and other forced convection heat transfer methods have been applied to the internal surface of turbine blade leading edge, among which impingement cooling is one of the most effective internal cooling methods, but its arrangement would weaken the blade structure strength [1]. Since film cooling is the only

method for blade external surface cooling. Thus impingement and film composite cooling are used extensively in gas turbine blades in recent years.

A decade ago, experimental study was the only way to obtain detailed and reliable heat transfer information about the turbulent, 3-dimensional flows in the complex impinging cooling flows. The early investigation on concave surface impingement cooling has been summarized by Chupp et al. [2], Metzger et al. [3-4], Bunker and Metzger [5], and they experimentally studied impingement cooling of concave surface through linear circular air jets, considering the effect of Reynolds number, target surface shape, jet spacing and size, jet arrangement, the number of jet holes and the distance between jet exit and target surface. Yang et al. [6] and Choi et al. [7] investigated impingement cooling on a semicircular concave surface. They identified the effects of nozzle shape and curvature or measured the distributions of mean velocity and velocity fluctuation on concave surface in free, impinging and wall jet flow regions and local Nusselt numbers variation with Reynolds numbers, jet spacing and spacing between the nozzle exit and the target surface. Wei et al. [8] found that rotation effects increase the serpentine cooling and reduce the jet impingement cooling.

Numerical investigations on the flow and heat transfer of impingement cooling on concave surfaces were first conducted by Kayansayan and Kucuka [9]. They compared numerical results with experimental data, and the findings show that the variation of the channel radius ratio could not affect the Nusselt number of the stagnation region, which is not in accordance with the results obtained by Choi et al. [7]. Taslim et al. [10-11], and Taslim and Bethka [12] investigated impingement cooling on concave surface under the influence of smooth and roughness wall, horseshoe ribs, jet to target wall spacing, exit flow schemes and crossflow. Their results indicated that heat transfer enhanced by roughness target surface, notched horseshoe, and horseshoe geometries, but reduced by the external crossflow. Souris et al. [13] studied impinging cooling on a semicircular concave surface and compared their numerical results with those from Choi et al. [7]. They found that maximum heat transfer occurs at $H/B = 6$ while Reynolds number is constant. An array of circular jets impinging on circular concave surface related to anti-icing system of aircraft wings was numerically studied by Fregeau et al. [14], who deduced dimensionless correlations between the average and the maximum Nusselt number and nozzle pitch, spacing of nozzle to target surface and hot air jet Mach number. Kumar and Prasad [15] studied the flow and heat transfer of a row of circular jets impinging on a concave surface, and they compared their numerical results with experimental results by Chupp et al. [2] and Bunker and Metzger [5]. The local pressure coefficient and Nusselt number variations along the concave plate are presented, and they found these values are about 12% below the available experimental data. Sharif and Mothe [16] numerically studied the effect of Reynolds number, surface curvature and nozzle to surface spacing on impingement cooling of concave cylindrical surface. Liu et al. [17-18] studied the effect of jet Mach number, jet spacing, jet size, and jet position on flow and heat transfer of turbine blade leading edge.

All papers cited above are about the effect of Reynolds number, jet diameter and spacing, jet to target surface distance, jet arrangement, target surface curvature and geometry without film coolant extraction. The addition of film cooling is expected to affect the heat transfer in the internal region of the impingement cooling since it changes the flow path of the coolant and reduce the cross flow. Only few of pervious works focus on impingement/film composite cooling. The first works was done by Hollworth and Dagan in 1980 [19], and they investigated impingement cooling with film coolant extraction on a plate. Then Metzger and Bunker [20] experimentally studied impingement cooling of concave surface through lines of circular air jets with and without film coolant extraction, and results shown that the flow extraction rate have smaller effect on heat transfer. Ekkad et al. [21] experimentally investigated impingement cooling on a target plate with film cooling holes, and results suggested that the film extraction reduces crossflow effects on jet impingement heat transfer. Taslim and Khanicheh [22,23], and Taslim and Khanicheh [24] investigated heat transfer of impingement cooling on concave surface with film holes under the influence of roughness target wall, jet nozzle geometry, showerhead and gill film holes. Their results indicated that heat transfer enhanced by roughness target surface and the showerhead film holes. Mouzon et al. [25], Ravelli et al. [26], Jonathan et al. [27] and Mathew et al. [28] investigated the effect of impingement cooling on film cooling of turbine blade leading edge, and the results showed that the overall film cooling effectiveness was only slightly improved by the impingement cooling. Liu et al. [29] studied the effect of blowing ratio and film hole spanwise angle on blade leading edge impingement and film composite cooling, and results indicate that heat transfer coefficient on the internal surface increases with blowing ratio, and slightly changes with film hole spanwise angle. But the external film cooling effectiveness distribution would vary rapidly with the blowing ratio and the film hole spanwise angle.

However, the previous works are focus on the influence of film extraction on impingement cooling, or the effect of flow condition on external film cooling, almost no attention was paid to the effects of main flow condition and impingement geometry parameters on the internal heat transfer and the external film cooling effectiveness of impingement and film composite cooling. In this study, the flow structure and heat transfer of the impingement and film composite cooling on turbine leading edge model is studied, and the effects of the attack angle and flat portion to jet nozzle diameter ratios are investigated.

2 Physical and Mathematical Models

2.1 Geometrical details

Figure 1 shows the leading edge model geometry structure. It is the same with the geometry used in experimental study of Maikell et al. [27] and in the computational study of Mathew et al. [28]. The film cooling configuration included three rows of holes positioned staggered along the stagnation line and at ±25º from the stagnation line, the impingement jets were directed to impact the internal surface in each stagnation film hole. The

geometrical dimensions of different jet configurations are listed in Table 1.

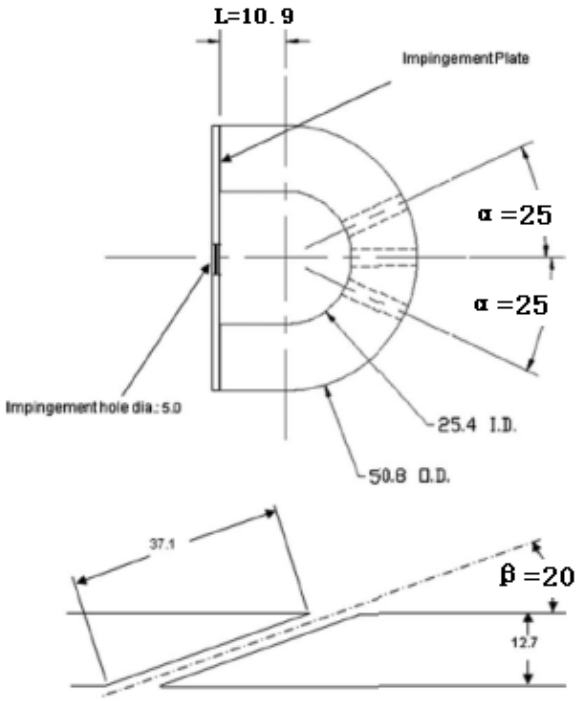

Fig. 1 Sketch of the leading edge model [27]

Table 1 Geometric detail of jet configurations

Dimension	*Values*
C (mm)	24.2
D_f (mm)	3.18
D_i (mm)	25.4
D_{ip} (mm)	5
D_o (mm)	50.8
L/D_{ip}	0.18, 1.18, 2.18, 3.18, 4.18
α (°)	25
β (°)	20

2.2 Numerical method

Boundary conditions and solution procedure

Boundary conditions are matched with those in References [27]. Periodic conditions were applied to minimize the computational effort, half leading edge was employed for cases of attack angle value with 0.0º (as shown in Fig.2), while whole leading edge adopted for case of attack angle not equal to 0.0º. The mainstream inlet air total temperature is 300K, velocity is 15m/s and turbulent intensity is 5%. The coolant inlet total temperature is 200K and turbulent intensity is 5%. Average static pressure at the outlet is 0.106MPa. The impingement target wall temperature is 235K, other walls are adiabatic and nonslip. The fluid is nitrogen (ideal gas). The convergence of simulation is achieved when the root mean square residuals of the momentum, mass equations, energy equation and turbulent equations are lower than 10^{-5} and remain steady.

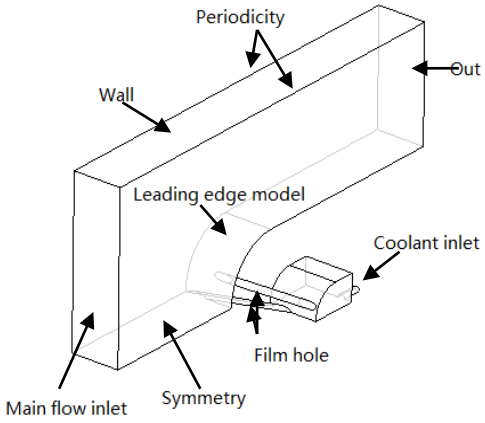

Fig. 2 Schematic of the computational domain and boundary condition

Mesh procedure

The numerical simulations are performed by using a commercial CFD software CFX11.0. The solutions are obtained by solving the steady compressible Reynolds averaged Navier-Stokes equations, in which the finite control volume method is applied to discretize these equations, and a second order form with high resolution correction is applied to discretize the convection term. The overall accuracy of the calculation is of the second order.

Commercial software Gambit 2.3.16 is adopted to generate the unstructured grids for the calculation domains. The mesh includes tetrahedral elements in the main flow passage and prism elements in the near wall regions, the jet nozzle, film hole and the grid nodes in and around its downstream are also refined. The low-Reynolds number standard k-ω model and SST k-ω model would require at least y^+<2. In this investigation, for standard k-ω model and SST k-ω model, the wall grid y^+ is less than 1.0, more than 15 cells were put into the boundary layer, and the total grid nodes is about 2.03 million. But for standard k-ε model and RNG k-ε model, the wall grid y^+ is in the range between 20 and 100, and the total grid nodes is about 1.91 millions. The ratio of cell size increases by about 30% outward from the walls in all cases. Figure 3 shows the grid generation result.

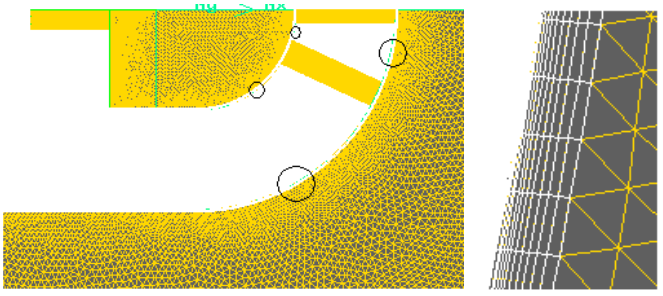

Fig. 3 Mesh (cross section)

Comparisons with available experimental data

In order to validate the ability of different turbulence models to represent flow and heat transfer of the present work,

first calculation of an experimental case investigated by Bunker and Metzger [5] is adopted as model verification for impingement cooling in this paper. Detailed geometry can be found in Reference [5]. The case with H/B=24, r*=1.0, Re=6750 and C/D_{ip}=4.67 is considered as a comparison. Calculations are carried out with three turbulence models, the RNG k-ε model, the standard k-ω model and the SST k-ω model. Figure 4 shows the comparison between predicted and available measured results including the spanwise area-weighted average Nusselt number along the target surface, and the model validation results by Kumar et al. [15]. The results demonstrated that the SST k-ω model is the best, and the maximum relative error is 13.58%. And details of the validation of turbulence models for the simulation of impingement cooling can be found in the previous works [17].

For a constant temperature surface, the local heat transfer coefficient can be expressed as

$$h = \frac{q_w}{T_w - T_c} \tag{1}$$

And the value of h can be normalized in the form of local Nusselt number as

$$Nu = \frac{hD_f}{\lambda} = \frac{q_w \cdot D_f}{(T_w - T_c)\lambda} \tag{2}$$

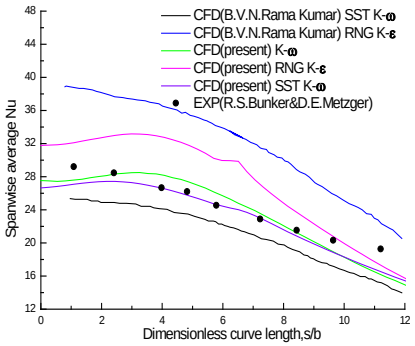

Fig.4 Comparison of spanwise-averaged Nusselt number along target plane with experimental results by Bunker and Metzger [5]

Then, a calculation of an experimental case investigated by Maikell et al. [27] is adopted as model verification for film cooling in the impingement and film composite cooling. Geometry and boundary conditions are the same with provided above. The case with M=1.0 (blowing ratio) and γ=0.0° (attack angle of mainstream flow, the definition of γ is shown in Fig.5) is considered as a comparison. Calculations are carried out with four turbulence models, the standard k-ε model, the RNG k-ε model, the standard k-ω model and the SST k-ω model.

Fig.5 Definition of γ

For an adiabatic surface, the local film cooling effectiveness can be expressed as

$$\eta = \frac{T_\infty - T_{aw}}{T_\infty - T_c} \tag{3}$$

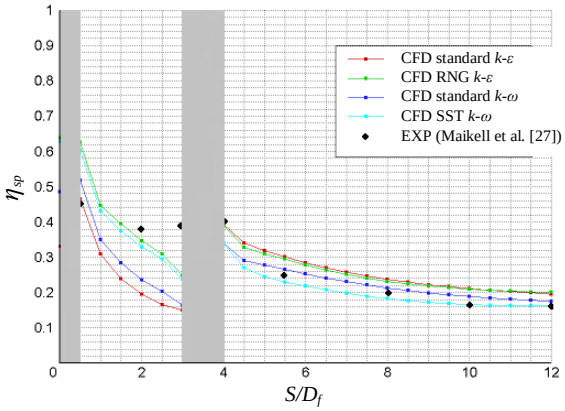

Fig.6 Comparison of spanwise-averaged film cooling effectiveness along leading edge with experimental results by Maikell et al. [27]

Figure 6 shows the comparison of the predicted spanwise-averaged film cooling effectiveness with the available measured results along the leading edge model. And Table 1 presents the mean relative error of the four different models from the experimental results by Maikell et al. [27]. The results demonstrated that the SST k-ω model is the best, and its mean relative error is 5.85% (as shown in Table 2). More details can be found in previous paper [29]. Since the relative error predicted by the SST k-ω model are the minimum one among the models both in impingement cooling case and in film cooling with impingement case, all the following results reported are based on SST k-ω model.

Table 2 Average relative error of different models from experimental results

Turbulence model	Average relative error
Standard k-ε	7.52%
RNG k-ε	6.34%
Standard k-ω	6.92%
SST k-ω	5.85%

Grid independence analysis

To save simulation time, half leading edge was employed for model validation and grid independence analysis, since the investigation domain is symmetrical when γ=0.0°. Then four different meshes with the grid node number of 0.91 million, 1.59 million, 2.03 million and 3.16 million were used to validate the grid independence. The mesh refinement has been synchronously imposed on every mesh in three coordinate directions. The SST k-ω turbulence model is employed, the wall y^+ is less than 1.0 and more than 15 cells were put into the boundary layer in all cases. The case with M=1.0 is adopted for grid independence test.

The area-weighted average Nusselt numbers on the leading edge internal surface and the area-weighted average film cooling effectiveness on the leading edge external surface obtained through the different meshes are demonstrated in Table 3 and Table 4 respectively [29]. The extrapolation value was

calculated by means of the Richardson Extrapolation method [30] with the results of 2.03 million nodes and 3.16 million nodes. A second order format with high resolution correction is applied to discretize the convection term in this paper. Therefore, based on the Roache's investigation, the average Nusselt number from the Richardson Extrapolation has a fourth order accuracy. Provided that these Nusselt number and cooling effectiveness are baseline solution, we can conclude that when the grid node number is larger than 2.03 million, increasing node number has a little effect on the value of error. In order to balance the calculation accuracy and the simulation time, about 2.03 million nodes were employed for half leading edge model. And as the investigation domain is no longer symmetrical when $\gamma \neq 0.0$, the whole leading edge was employed for cases$\gamma \neq 0.0$, and the total grid nodes is 4.07 million for those cases.

Table 3 Average Nusselt number on impingement target surface

Node number (million)	*average Nu*	*Relative error*
0.91	10.59	6.27%
1.59	10.14	1.71%
2.03	10.02	0.54%
3.16	10.00	0.35%
Extrapolation	9.97	-

Table 4 Average film cooling effectiveness on external surface

Node number (million)	*average η*	*Relative error*
0.91	0.1484	-2.33%
1.59	0.1450	-1.27%
2.03	0.1509	-0.66%
3.16	0.1512	-0.49%
Extrapolation	0.1519	-

3 Results and Discussions

The main flow attack angle have a significant effect on the flow pattern of the film cooling, and would affect the flow of the internal impingement cooling, so they are critical to the flow and heat transfer of the impingement and film composite cooling. In order to study its effects, numerical simulations are carried out at five different γ, values with 0.0^o, 0.5^o, 1.0^o, 3.0^o, 5.0^o, and five different L/D_{ip}(flat portion to jet nozzle diameter ratios), values with 0.18, 1.18, 2.18, 3.18, 4.18.

For a convenient analysis, it is suggested that the film hole positioned along the stagnation line will be numbered No.1, and the other numbered No.2.

3.1 Effect of γ

To investigate the effects of angle γ on impingement and film composite cooling of turbine leading edge, an analysis was done under the conditions of five different γ, values 0.0^o, 0.5^o, 1^o, 3^o, and 5^o for a fixed L/D_{ip}, 2.18, M, 1 and constant β, 20^o. And a detailed analysis was made for cases with γ values 0.5^o, 1^o, 3^o, and 5^o. As the investigation domain is no longer symmetrical when $\gamma \neq 0.0$, the whole leading edge was employed for cases $\gamma \neq 0.0$, and the total grid nodes is 4.07 million for those cases.

Flow fields

Figure 7 shows streamlines and contours of velocity magnitude on horizontal cross-sections at the center of film holes No.1 and No.2 in different γ. It can be observed that the flow field was approximately symmetric in the case of $\gamma = 0.5°$, while with an increase in γ, the flow pattern is no longer symmetrical, as the suppression of the mainstream flow on the two side film hole is not uniform anymore when $\gamma \neq 0.0$, and the different enhanced with the increases of γ.

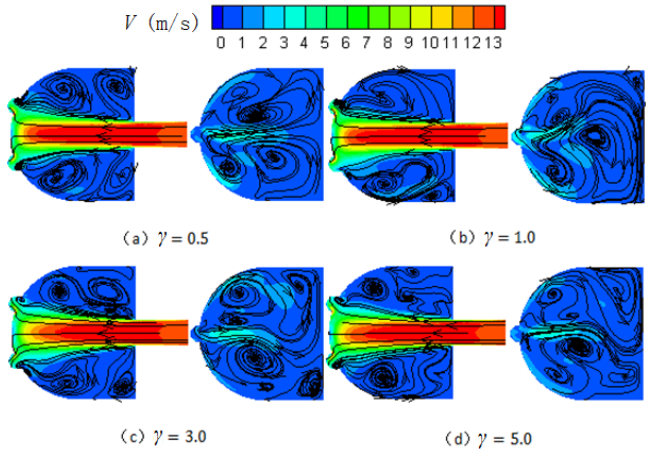

Fig. 7 Streamlines and contours of velocity magnitude on horizontal cross-sections at the center of film hole No.1 and No.2 in different γ

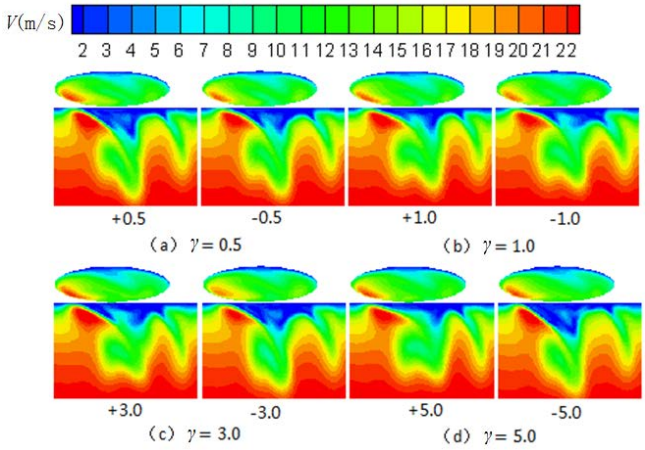

Fig. 8 Relative velocity magnititude on tangential section of film hole No.2 outlet for different values of γ

Figure 8 presents the velocity magnitude on tangential section of film hole No.2 outlet in different values of γ, the bottom side is the downstream of the main flow, and the left side is the upside of the film hole, as shown in Fig.9. It can be seen that the relative velocity distribution in hole No.2 hardly changes and its varying trend was exactly similar at varying γ. Additionally, velocity in down-left side of film hole No.2 is higher, while in the opposite is lower. The relative velocity

distribution trends in hole No.2 is almost uniform, and high velocity region on the positive γ side would enlarge with γ, while the high velocity region on the negative γ side reduces, which resulted from the flow field at the cooling hole exit on the negative attack angle side suppressed more strongly by main stream with the increase of inlet incidence angle. The low momentum region decreases and the velocity become uniform on the tangential section with an increasing in γ.

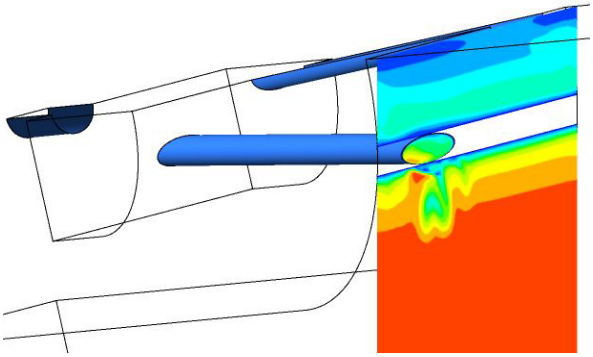

Fig.9 Sketch of tangential section of film hole No.2 outlet

Heat transfer

Figure 10 exhibits the Nusselt number contours of the internal impingement target surface for various values of γ. The *Nu* on the target surface barely changes at γ=0.5° and 1.0°. But while γ increases up to 3.0° or 5.0°, the *Nu* increase. This may be caused by the change of flow field of the impingement chamber as shown in Fig.7.

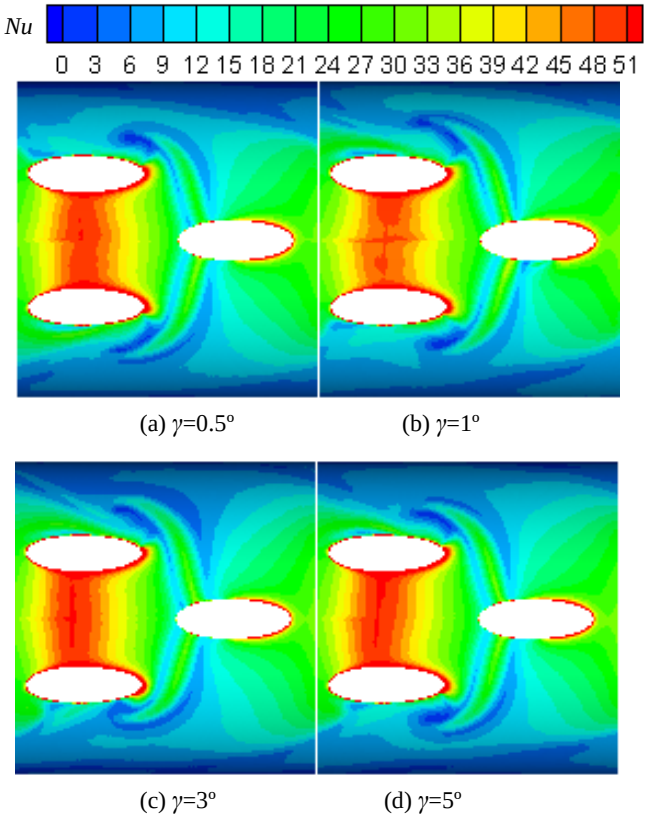

(a) γ=0.5° (b) γ=1°

(c) γ=3° (d) γ=5°

Fig. 10 *Nu* contours of the target surface in different γ

Film cooling effectiveness

Figure 11 indicates film cooling effectiveness contours of the leading edge surface in different γ, with results in two periods. It can be observed that the high cooling effectiveness region near the leading edge would move towards the positive attack angle side gradually with an increase of γ. This is attributed to the attack angle which will change the location of stagnation line, and the location will be shifted to the negative attack angle side with an increasing γ, thus causing the coolant mass flow rate from film holes No.1 flowing to the positive attack angle side be larger than that to the negative attack angle side. With the increase of γ, the region with highest η near the cooling hole No.2 on the positive attack angle side decreases, but the region with relatively high η is enlarged, while the variation of the area with highest η and with relatively higher η on the negative attack angle side is just on the contrary. That may be caused by the suppression of mainstream on coolant, and the suppression on negative attack angle side is stronger, which will lead the coolant flow from hole No.2 cover the wall well, and then high cooling effectiveness region are enlarged, but the coolant will be concentrated and the spanwise velocity dissipated quickly, thus the relatively high η region reduces.

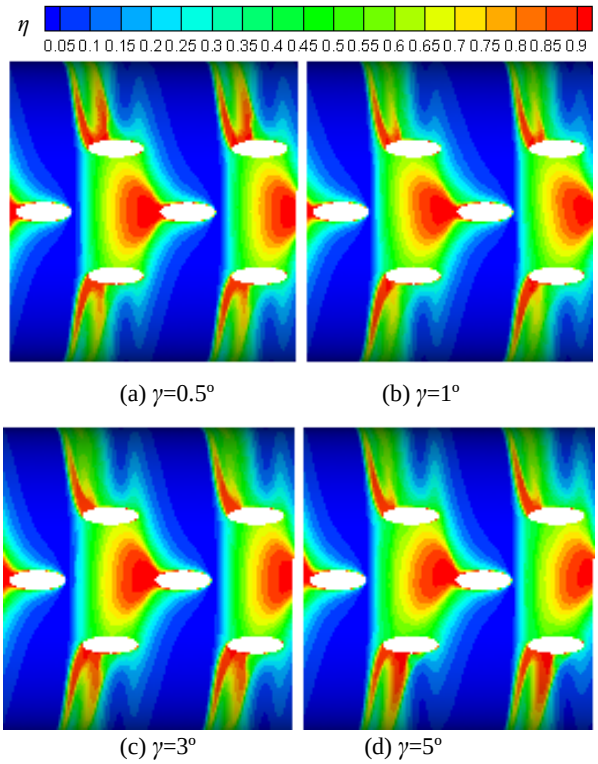

(a) γ=0.5° (b) γ=1°

(c) γ=3° (d) γ=5°

Fig. 11 Film cooling effectiveness contours in different γ

Figure 12 shows the spanwise-averaged film cooling effectiveness of the leading edge in different γ. Behind film hole No.2 (S/D_f>4), while γ<3.0°, the η_{sp} distribution is almost the same to each other, which is due to the slight change of the location of the stagnation line at low incidence angles, but while γ adds up to 5.0°, the η_{sp} on positive attack angle side increases rapidly and on negative incidence angle side decreases quickly.

Cooling effectiveness on both sides of film hole No.1 is sensitive to the variation of the leading edge stagnation line. For the three rows film holes ($0.5 \leqslant |S/D_f| \leqslant 3$), on the positive attack angle side, η_{sp} increases with γ, while η_{sp} on the negative attack angle side decreases with an increase in γ, which was attributed to the increasing coolant flow in the positive attack angle side from film hole No.1 due to the attack angle, and this would improve the cooling performance.

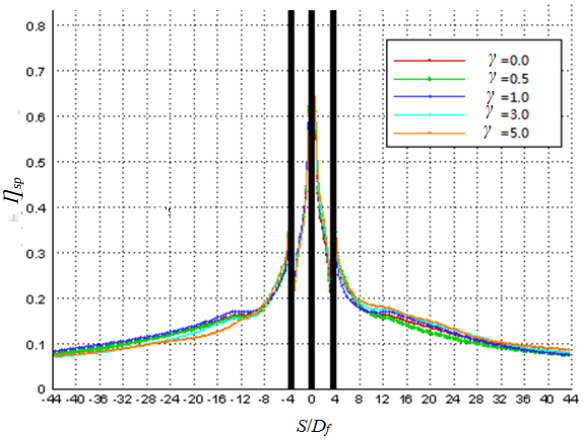

(a) Whole leading edge external surface

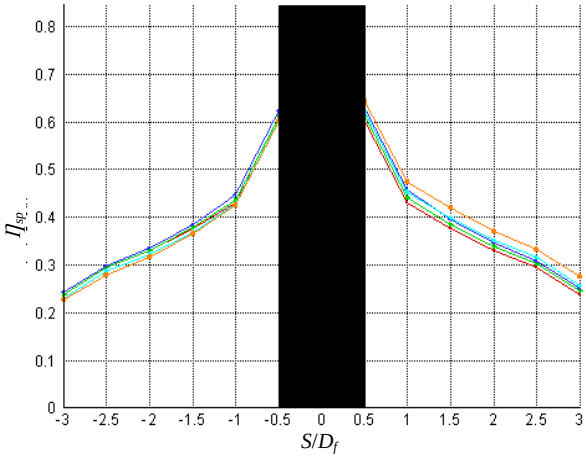

(b) Between the three rows of film holes ($0.5 \leqslant |S/D_f| \leqslant 3$)

Fig. 12 Spanwise-averaged film cooling effectiveness in different γ

3.2 Effect of L/D_{ip}

To investigate the effects of ratio of jet to target distance to jet nozzle diameter on impingement and film composite cooling of turbine leading edge, an analysis was done under the conditions of five different L/D_{ip}, values with 0.18, 1.18, 2.18, 3.18, 4.18 and for a fixed γ, 0.0°, M, 1 and constant β, 20°. And a detailed analysis was made for cases with L/D_{ip}, values with 0.18, 1.18, 3.18 and 4.18. As the investigation domain is symmetrical when γ=0.0, a half leading edge was employed, and the total grid nodes is 2.03 million for those cases.

Flow fields

Figure 13 presents streamlines and contours of velocity magnitude on horizontal cross-sections at the center of film holes No.1 and No.2 for various values of L/D_{ip}, 0.18, 1.18, 3.18 and 4.18. With an increase of L/D_{ip}, velocity near the stagnation region on the target surface decreases, but area of stagnation region increases. Scale of Kelvin–Helmholtz vortices increases, but its strength drops down, that means the two sides wall will be scoured by the Kelvin–Helmholtz vortices with a larger region but a weaker intensity.

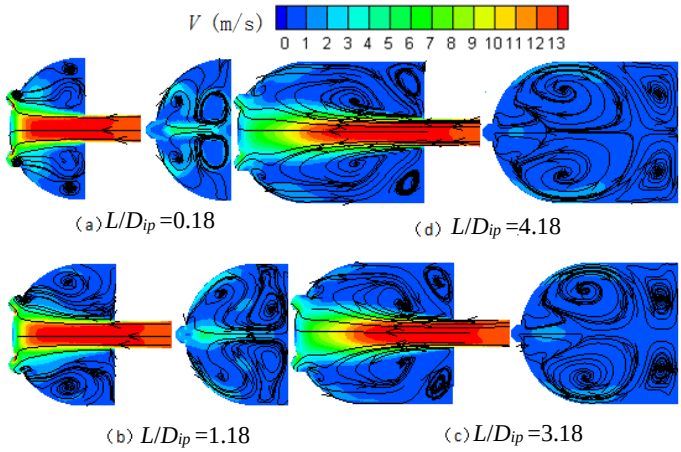

Fig. 13 Streamlines and contours of velocity magnitude on horizontal cross-sections at the center of film hole No.1 and No.2 for various values of L/D_{ip}

Flow rate and average blowing ratio of film holes No.1 and No.2 for various values of L/D_{ip} is shown in Tab.5. It can be seen from the table that the flow rate and the average blowing ratio in film hole No.1 is higher than that of film hole No.2. This is because velocity of the film hole No.2 is lower for its inlet is farther away from stagnation region compare to film hole No.1. However, the flow rate and the average blowing ratio of film hole No.1 increase slightly with L/D_{ip}, while those of film hole No.2 decrease slightly. Therefore, it can be obtain that L/D_{ip} has little influence on the coolant distribution.

Table 5 Flow rate and average blowing ratio of film holes No.1 and No.2 for various values of L/D_{ip}

L/D_{ip}	m_1	m_1%	M_{1av}	m_2	m_2%	M_{2av}
0.18	0.1627	76.02	1.1434	0.1026	23.98	0.7210
1.18	0.1639	76.60	1.1518	0.1002	23.40	0.7041
2.18	0.1658	77.47	1.1651	0.0964	22.53	0.6774
3.18	0.1661	77.61	1.1673	0.0958	22.39	0.6732
4.18	0.1663	77.67	1.1687	0.0956	22.33	0.6718

Heat transfer

Figure 14 exhibits the Nusselt number contours of the internal impingement target surface for various values of L/D_{ip}, with results in whole leading edge inner surface. It can be seen that with an increases in L/D_{ip}, the value of highest Nusselt number decreases but the area of high Nusselt number increases. This is because that stagnation velocity decreases and stagnation region area increases with increases of L/D_{ip}, the erosion strength of cooling jet was weaken as analyzed in Fig.13. But the high Nusselt number region between two stagnation region barely changes with L/D_{ip}.

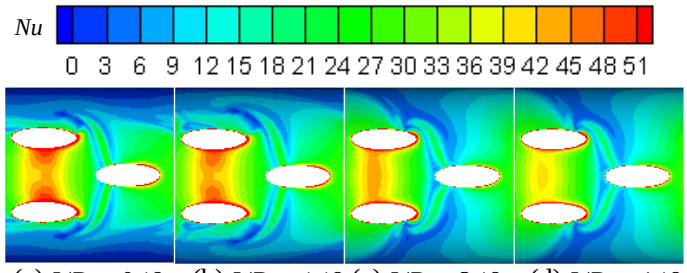

(a) L/D_{ip} =0.18 (b) L/D_{ip} =1.18 (c) L/D_{ip} =3.18 (d) L/D_{ip} =4.18

Fig. 14 *Nu* contours of the target surface for various values of L/D_{ip}

Film cooling effectiveness

Contours of film cooling effectiveness for various values of L/D_{ip} are given on Fig.15, with results in two periods and whole leading edge external surface. With an increase in L/D_{ip}, no obvious changes can be found in high film cooling effectiveness region for film hole No.2. But for film hole No.1, area of the highest cooling effectiveness region decreases continually. This may because in cases of lower L/D_{ip} values, blowing ratio of film hole No.1 is lower while coolant is more inclined to flow along the blade external surface, and coolant film turbulence intensity is higher, then cooling effectiveness around and downstream the film hole can be improved under the strong turbulence for the coolant flow from film hole dissipated quicker. In addition, L/D_{ip} has little effect on the distribution of cooling effectiveness far behind film hole.

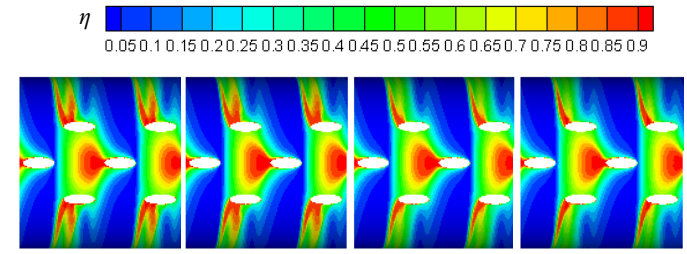

(a) L/D_{ip} =0.18 (b) L/D_{ip} =1.18 (c) L/D_{ip} =3.18 (d) L/D_{ip} =4.18

Fig. 15 Film cooling effectiveness contours in different L/D_{ip}

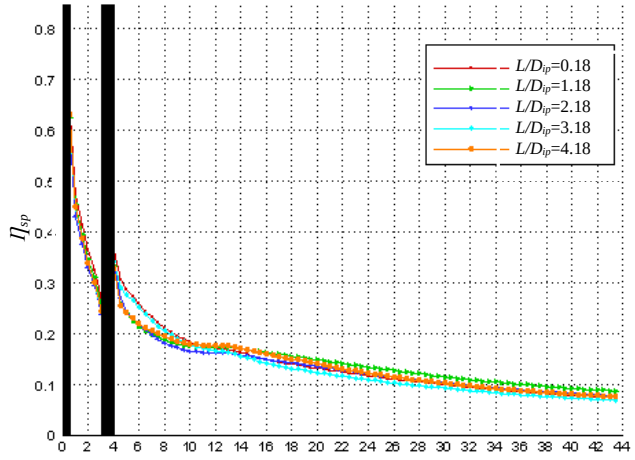

Fig. 16 Spanwise-averaged film cooling effectiveness for various values of L/D_{ip}

Figure 16 shows spanwise-averaged film cooling effectiveness of the leading edge for various values of L/D_{ip}. It can be found that spanwise-averaged film cooling effectiveness increases with L/D_{ip} in region $S/D_f \leqslant 3.0$. And L/D_{ip} has little impact on the distribution of spanwise-averaged film cooling effectiveness at when $S/D_f \geqslant 10.0$, and in that region the distribution of spanwise-averaged film cooling effectiveness becomes even.

5 Conclusions

In this study, a numerical simulation has been performed to study the flow and heat transfer of the impinging and film composite cooling on turbine blade leading edge, and the influence of the main flow attack angle and five flat portion to jet nozzle diameter ratios on blade leading edge impingement and film composite cooling has been analyzed.

Different turbulence models are validated and results show that the SST k-ω model is the best for solution of the present problem. And a grid refinement study shows that 2.03 million grid nodes could ensure about 0.54% relative error on internal impingement cooling and -0.66% relative error on external film cooling for the half model.

With an increase of attack angle, the coolant distribution from film hole No.1 varies, the Nusselt number on the internal target surface increases slightly, and the area of the high film cooling effectiveness region near the cooling hole No.2 on the positive attack angle side decreases, but the region with relatively high film cooling effectiveness is enlarged, while the variation of the region with highest film cooling effectiveness and relatively higher film cooling effectiveness on the negative attack angle side with an increase of attack angle is just on the contrary.

With an increase of flat portion to jet nozzle diameter ratio, the flow rate and the average blowing ratio of film hole No.1 increase slightly, while those of film hole No.2 decrease slightly. At internal surface, the value of highest Nusselt number decreases but the area of high Nusselt number increases. And at external surface, area of highest film cooling effectiveness region of film hole No.1 decrease slightly.

Acknowledgments

This work is supported by China Postdoctoral Science Foundation (Grant No. 2013M542345), Natural Science Basic Research Plan in Shaanxi Province of China (Grant No.2014JQ7286) and The Fundamental Research Funds for the Central Universities..

References

[1] Han J.C., Dutta S., Ekkad S.V., Gas Turbine Heat Transfer and Cooling Technology, Taylor & Francis, New York, 2000.

[2] Chupp R.E., Helms H.E., McFadden P.W., Brown T.R., Evaluation of Internal Heat Transfer Coefficients for Impingement Cooled Turbine Airfoils, Journal of Aircraft, 1969, 6:203-208.

[3] Metzger D.E., Yamashita T., Jenkins C.W., Impingement Cooling of Concave Surface With Lines of Circular Air Jets, ASME Journal of Engineering for Power, 1969, 91:149-158.

[4] Metzger D.E., Baltzer R.T., Jenkins C.W., Impingement Cooling Performance in Gas Turbine Airfoils Including Effects of Leading

Edge Sharpness, ASME Journal of Engineering for Power, 1972, 94:219-225.
[5] Bunker R.S., Metzger D.E., Local Heat Transfer in Internally Cooled Turbine Airfoil Leading Edge Regions: Part I — Impingement Cooling Without Film Coolant Extraction, ASME Journal of Turbomachinery, 1990, 112:451-458.
[6] Yang G., Choi M., Lee J.S., An Experimental Study of Slot Jet Impingement Cooling on Concave Surface: Effects of Nozzle Configuration and Curvature, International Journal of Heat and Mass Transfer, 1999, 42: 2199-2209.
[7] Choi M., Yoo H.S., Yang G., Lee J.S., Sohn D.K., Measurements of Impinging Jet Flow and Heat Transfer on a Semi-circular Concave Surface, International Journal of Heat Mass Transfer, 2000, 43:1811-1822.
[8] Wei H., Chiang D., Li H. L., Jet Impingement and Forced Convection Cooling Experimental Study in Rotating Turbine Blades, Proceedings of the ASME Turbo Expo, 2009, GT2009-59795.
[9] Kayansaya N., Kucuka S., Impingement Cooling of a Semi-cylindrical Concave Channel by Confined Slot-air-jet, Experimental Thermal and Fluid Science , 2001, 25:383-396.
[10] Taslim M.E., Setayeshgar L., Spring S.D., An Experimental Evaluation of Advanced Leading Edge Impingement Cooling Concepts, ASME Journal of Turbomachinery, 2001, 123:147-153.
[11] Taslim M.E., Bakhtari K., Liu H., Experimental and Numerical Investigation of Impingement on a Rib- Roughened Leading Edge Wall, ASME Journal of Turbomachinery, 2003, 125:682-691.
[12] Taslim M.E., Bethka D., Experimental and Numerical Impingement Heat Transfer in an Airfoil Leading-Edge Cooling Channel With Cross-Flow, ASME Journal of Turbomachinery, 2009, 131:011-021.
[13] Souris N., Liakos H., Founti M., Impinging Jet Cooling on Concave Surfaces, AICHE Journal, 2004, 50:1672-1683.
[14] Frageau M., Saeed F., Paraschivoiu I., Numerical Heat Transfer Correlation for Array of Hot-Air Jets Impinging on 3-dimensional Concave Surface, Journal of Aircraft, 2005, 42:665-670.
[15] Kumar B.V.N.R., Prasad B.V.S.S.S., Computational Flow and Heat Transfer of a Row of Circular Jets Impinging on a Concave Surface, Heat Mass Transfer, 2008, 4:667-678.
[16] Sharif M.A.R., Mothe K.K., Parametric Study of Turbulent Slot-Jet Impingement Heat Transfer from Concave Cylindrical Surfaces, International Journal of Thermal Sciences, 2010, 49:428-442.
[17] Liu Z., Feng Z.P., Song L.M., Numerical Study of Flow and Heat Transfer of Impingement Cooling on Model of Turbine Blade Leading Edge, ASME Turbo Expo, 2010, GT2010-23711.
[18] Liu Z., Feng Z.P., Numerical Simulation on the Effect of Jet Nozzle Position on Impingement Cooling of Gas Turbine Blade Leading Edge, International Journal of Heat and Mass Transfer, 2011, 54(23-24):4949~4959.
[19] Hollworth, B.R., Dagan L., Arrays of Impingement Jets with Spent Fluid Removal through Vent holes on the Target Surface, Part I: Average Heat Transfer, Journal of Engineering for Power, 1980, 102: 994-999.
[20] Metzger D.E., Bunker R.S., Local Heat Transfer in Internally Cooled Turbine Airfoil Leading Edge Regions: Part II — Impingement Cooling With Film Coolant Extraction, ASME Journal of Turbomachinery, 1990, 112: 459–466.
[21] Ekkad S.V., Huang Y., Han J.C., Impingement Heat Transfer on a Target Plate with Film Holes, Journal of Thermophysics and Heat Transfer, 1999, 13(4): 522-528.
[22] Taslim M.E., Pan Y, Spring S.D., An Experimental Study of Impingement on Roughened Airfoil Leading-Edge Walls with Film Holes, ASME Journal of Turbomachinery, 2001, 123(4): 766-773.
[23] Taslim M.E., Pan Y, Bakhtari K., Experimental racetrack shaped jet impingement on roughened leading edge wall with film holes, ASME Turbo Expo, 2002, GT2002-30477.
[24] Taslim M.E., Khanicheh A., Experimental and Numerical Study of Impingement on an Airfoil Leading Edge With and Without Showerhead and Gill Film Holes, ASME Journal of Turbomachinery, 2006, 128 (2): 310-320.
[25] Mouzon B.D., Terrel E.J., Albert J E., Bogard D.G., Net Heat Flux Reduction and Overall Effectiveness for a Turbine Blade Leading Edge, ASME Turbo EXPO, 2005, GT2005-69002.
[26] Ravelli S., Dobrowolski L., Bogard D.G., Evaluating the Effects of Internal Impingement Cooling on a Film Cooled Turbine Blade Leading Edge, ASME Turbo EXPO, 2010, GT2010-23002.
[27] Maikell J., Bogard D.B., Piggush J., et al., Experimental Simulatin of a Film Cooled Turbine Blade Leading Edge Including Thermal Barrier Coating Effects, ASME Journal of Turbomachinery, 2011, 133(1), 011014:1-7.
[28] Mathew S., Ravelli S., Bogard D.G., Evaluation of CFD Predictions Using Thermal Field Measurements on a Simulated Film Cooled Turbine Blade Leading Edge, ASME Journal of Turbomachinery, 2013, 135(1):011021:1-10.
[29] Liu Z., Ye L., Wang C.Y., Feng Z.P., Numerical Simulation on Impingement and Film Composite Cooling of Blade Leading Edge Model for Gas Turbine, Applied Thermal Engineering, 2014, 73(2): 1432-1443.
[30] Roache, P.J., Perspective: a method for uniform reporting of grid refinement studies, Journal of Fluids Engineering, 1994, 116: 405-413.